

**GT2004-53867**

## **ROLE OF TIP-LEAKAGE VORTICES AND PASSAGE SHOCK IN STALL INCEPTION IN A SWEEPED TRANSONIC COMPRESSOR ROTOR**

Chunill Hah  
NASA Glenn Research Center,  
MS 5-11, Cleveland, Ohio 44135  
216-433-6377, chunill.hah@grc.nasa.gov

Douglas C. Rabe  
U.S. Air Force, Air Force Research Laboratory  
WPAFB, Ohio 45433-6523  
937-255-6801, douglas.rabe@wpafb.af.mil

Aspi R. Wadia  
GE Aircraft Engines  
One Neumann Way, Cincinnati, Ohio 45215-6301  
513-243-3504, aspi.wadia@ae.ge.com

### **ABSTRACT**

The current paper reports on investigations aimed at advancing the understanding of the flow field near the casing of a forward-swept transonic compressor rotor. The role of tip clearance flow and its interaction with the passage shock on stall inception are analyzed in detail. Steady and unsteady three-dimensional viscous flow calculations are applied to obtain flow fields at various operating conditions. The numerical results are first compared with available measured data. Then, the numerically obtained flow fields are interrogated to identify the roles of flow interactions between the tip clearance flow, the passage shock, and the blade/endwall boundary layers. In addition to the flow field with nominal tip clearance, two more flow fields are analyzed in order to identify the mechanisms of blockage generation: one with zero tip clearance, and one with nominal tip clearance on the forward portion of the blade and zero clearance on the aft portion.

The current study shows that the tip clearance vortex does not break down, even when the rotor operates in a stalled condition. Interaction between the shock and the suction surface boundary layer causes the shock, and therefore the tip clearance vortex, to oscillate. However, for the currently investigated transonic compressor rotor, so-called breakdown of the tip clearance vortex does not occur during stall inception.

The tip clearance vortex originates near the leading edge tip, but moves downward in the spanwise direction inside the blade passage. A low momentum region develops above the tip clearance vortex from flow originating from the casing boundary layer. The low momentum area builds up immediately downstream of the passage shock and above the core vortex. This area migrates toward the pressure side of the blade passage as the flow rate is decreased. The low momentum area prevents incoming flow from passing through the pressure side of the

passage and initiates stall inception. It is well known that inviscid effects dominate tip clearance flow. However, complex viscous flow structures develop inside the casing boundary layer at operating conditions near stall.

### **INTRODUCTION**

It is well known that a large portion of aerodynamic loss in modern transonic compressors occurs near the rotor tip section. Complex flow structures near the casing arise from interactions between the tip clearance flow, passage shock, and blade boundary layers and often limit the operating range. Numerous experimental and analytical studies of endwall flow structures in transonic compressors have been reported (for example, Adamczyk et al. [1993], Copenhaver et al. [1996], Hah and Loellbach [1999], Chima [1998], Suder and Celestina [1994], Van Zante et al. [2000], Rabe and Hah [2002]). Although many details of the end wall flow structure in transonic compressors have emerged from these studies, the precise flow mechanisms that lead to stall inception, especially the role of the tip clearance vortex, are not clearly understood.

Recently, various studies (for example, Schlechtriem and Loetzerich [1997], Hoffmann and Ballmann [2003], Yamada et al. [2003]) have proposed tip clearance vortex breakdown as a possible cause of stall initiation in a conventionally designed rotor. Vortex breakdown is referred to as a phenomenon in which an abrupt change in the vortex core structure occurs. In transonic compressors, it is argued that shock/tip-vortex interaction can cause vortex breakdown. Thomer et al. [2002] studied the interaction between longitudinal vortices and normal and oblique shocks. They proposed criteria for the occurrence of vortex breakdown from their study. In a typical transonic compressor near the stall condition, the tip core vortex is oblique to the passage shock and the swirl intensity of the core

vortex seems too weak for vortex breakdown based on the criteria proposed by Thomer et al. [2002]. In the present study, the behavior of the tip clearance core vortex in the current rotor was studied first to identify any break-up during stall. Because no break up of the tip clearance core vortex occurred, the origin of blockage near the casing during stall was further examined.

Both He and Ismael [1997] and Hah and Rabe [2001] studied stall inception in transonic compressor rotors numerically. He and Ismael [1997] calculated 8 out of 36 blade passages of NASA's Rotor 37 to simulate rotating stall inception. Hah and Rabe [2001] performed full-annulus calculations to investigate stall inception in a modern high-tip-speed transonic compressor rotor. Both of these simulations used relatively coarse computational grids to accommodate multi-passage unsteady viscous flow simulations; therefore, detailed flow structures inside the casing boundary layer were not fully resolved. However, both studies revealed that the stall process in an isolated transonic compressor rotor is different from that in a subsonic compressor rotor. In an isolated transonic compressor rotor, the passage shock suppresses upstream propagation of flow disturbances near the tip outside the wall boundary layers. As a result, variations in flow structure between blade passages are less pronounced in stalled transonic rotors than in stalled subsonic rotors. For the present study, a single-passage flow simulation is used to study the interaction between the tip clearance core vortex and the passage shock. While a single-passage flow analysis cannot simulate asymmetric features of the flow in the stalled condition, it can be used to examine detailed behavior of the tip clearance core vortex and its interaction with the passage shock during stall at transonic operating conditions.

The concept of a swept transonic rotor has been introduced in the design of highly loaded, high-through-flow, transonic compressors to retain aerodynamic efficiency and operating range with the increasing rotor tip speed (for example, Wennerstrom and Puterbaugh [1984]). Both measurements and numerical studies have shown that a forward-swept rotor has a larger stall margin and higher efficiency than a similar radially stacked rotor (Wadia et al. [1997], Hah et al. [1998]). Detailed studies of endwall flow structures in swept compressor rotors operating near stall have not yet been reported.

The primary objectives of the current work are as follows:

1. To investigate detailed flow structures in the endwall region, including interactions between the tip clearance flow, passage shock, and blade boundary layers.
2. To examine the behavior of the tip clearance vortex during stall inception.
3. To recommend future research efforts in controlling endwall flow behavior in transonic compressors.

## FORWARD-SWEPT ROTOR

Figure 1 shows a three-dimensional view of the forward-swept rotor investigated in the current study. The rotor was designed to improve the performance of an already well-designed radially stacked rotor through aerodynamic sweep.

The key design parameters of the rotor are given in Table 1. The rotor was swept forward using both chord barreling and tangential lean in the direction of rotation. The design procedure was identical to that used to design unswept rotors and is presented by Wadia and Law [1993]. The rotor was tested at the Compressor Aerodynamic Research Laboratory (CARL) at Wright Patterson Air Force Base (WPAFB). Details of the setup, instrumentation, and experimental uncertainties are described by Law and Wadia [1993]. Experimental instrumentation included flow measurements at the stage inlet and exit, instrumentation for total pressure and total temperature at the downstream stator leading edge, and steady and dynamic pressure measurements along the rotor casing. Rotor running geometry and measured tip clearance of 0.02 inches are used for the numerical analysis. Therefore, deflections of the rotor geometry at running speed were properly accounted for in the numerical simulations.

## NUMERICAL PROCEDURE AND COMPUTATIONAL GRID

Steady and unsteady, three-dimensional, Reynolds-averaged Navier-Stokes equations were solved to obtain steady and unsteady flow fields at various operating conditions. Unsteady solutions were used to identify movement of the tip clearance vortex at stable operating conditions and to obtain instantaneous flow structures during stall inception.

In the current study, the governing equations are solved with a pressure-based implicit method using a fully conservative control volume approach. A modified two-equation turbulence model is applied for turbulence closure. A third-order accurate interpolation scheme is used for the spatial discretization of convection terms and central differencing is used for diffusion terms. The method is of second-order spatial accuracy on smoothly varying grids. For time-dependent terms, an implicit second-order scheme is used and a number of sub-iterations are performed at each time step. Previous studies using the current numerical code indicate that aerodynamic losses in a typical transonic compressor are predicted well enough for engineering guidance in design applications. Also, the qualitative stall range is calculated reasonably well with the numerical code. Details of the current method and applications to transonic flows are given by Hah and Wennerstrom [1991].

The computational grid is shown in Fig. 1. A single blade passage consists of 198 nodes in the blade-to-blade direction, 77 nodes in the spanwise direction, and 280 nodes in the streamwise direction. The rotor tip clearance geometry is accurately represented by 28 nodes in blade-to-blade direction, 30 nodes in the spanwise direction, 185 nodes in the streamwise direction. The I-grid topology is used to reduce grid skewness, and a single-block grid is used for the main passage and the tip clearance.

Standard boundary conditions for isolated rotor flow were applied at the boundaries of the computational domain. Non-reflecting boundary conditions were applied at the inlet and the exit. Periodicity conditions were applied at the periodic

surfaces, and no-slip conditions were used on solid walls. A previous study by Copenhaver et al. [1997] showed that a time step of 0.00025 sec. was necessary to capture shock motion in a similar transonic rotor. For the present study, the unsteady nature of the flow originates primarily from the interaction of the shock with the blade boundary layer and the resulting vortex shedding. Therefore, a time step of 0.0000125 sec. was used for all unsteady flow simulations.

## COMPARISON WITH MEASURED DATA

Measured and calculated rotor performance maps are presented in Fig. 2. Calculations were performed with the nominal tip clearance and with zero tip clearance. Additional calculations were performed near the stall condition for a partial clearance case with nominal clearance on the forward 40% chord and zero clearance on the aft 60% chord. Compared to the measurements, the present numerical procedure calculates a slightly higher pressure rise and a slightly lower adiabatic efficiency for the current compressor. The measured rotor characteristics are derived from measurements downstream of the stator. No attempts were made to obtain better agreement with the measurements. Previous studies on a similar rotor (Copenhaver et al. [1996]) showed that the current numerical procedure represents measured flow characteristics well enough for this type of investigation. With zero clearance, the efficiency increases by about 1.2%. This difference is close to the findings of L. H. Smith [1970] and agrees with a previous study on the effects of tip clearance on the performance of a transonic compressor rotor (Copenhaver et al. [1996]). Also with zero clearance, the stall margin increases by about 20%. Differences in efficiency and stall margin between the zero clearance and the nominal clearance cases represent the net effects of tip clearance. The partial tip clearance case exhibits an increase in stall margin of about 5% with no increase in efficiency.

For the nominal clearance case, the near-stall operating point corresponds to the highest backpressure at which a stable, steady, numerical solution can be obtained with a fixed exit static pressure. To identify the near-stall operating condition, the back pressure was increased by increments of 0.01 psi near the stall limit until a solution could no longer be obtained. To understand changes in flow structure during the stall process, an unsteady calculation was performed with a raised backpressure. An instantaneous solution from this calculation is identified in Fig. 2 as an in-stall condition. Further unsteady calculations were also performed at the near-stall condition to investigate the unsteady nature of interactions between the tip clearance flow, the passage shock, and the blade boundary layers.

Measured and calculated time-averaged pressure contours on the casing for the nominal clearance case are compared in Figs. 3 and 4. The results indicate that the numerical procedure calculates the overall flow structure correctly at different flow conditions. Therefore, numerical solutions at different operating conditions can be analyzed in detail to study the roles of the tip clearance vortex and the passage shock in stall inception for the present forward-swept rotor.

## Flow Structure with Zero Tip Clearance

To isolate effects of tip clearance flow in stall inception, a flow field with zero tip clearance was investigated first. Although the tip clearance was effectively set to zero, the casing remained stationary with relative motion between the rotor and the casing. Figures 5 and 6 show Mach number contours and velocity vectors near the leading edge at the near-stall operating condition. The results show that the boundary layer on the blade suction surface separates downstream of the passage shock. Strong cross flow from the suction surface to the pressure surface immediately downstream of the shock results in separation of the end wall boundary layer. Consequently, the flow incidence near the leading edge increases drastically. Previous studies on compressor stall phenomena (for example, Rabe and Hah [2002]) indicate that stall initiates when tip clearance flow spills into the adjacent blade passage from the pressure side at the leading edge. The results in Fig. 6a show that high flow incidence results from strong cross flow downstream of the passage shock where the end wall boundary layer separates and a large blockage is formed. Results in Fig. 6 also indicate that the increase in flow incidence is largest near the endwall and that stall initiates very close to the casing, not away from the casing.

## Flow Structure with Nominal Tip Clearance

Figure 7 shows entropy contours on several axial planes at three operating conditions. Three-dimensional traces of the tip clearance vortex are also shown. The tip vortex traces are formed by releasing particles from the region 1% chord downstream of the leading edge and 5% normalized tip clearance above the blade tip. The tip clearance vortices are maintained and so-called vortex breakdown is not observed, even at the in-stall operating condition. Various previous studies (for example, Schlechtriem and Loetzerich [1997], Hoffmann and Ballmann [2003], Yamada et al. [2003]) have indicated that tip clearance vortex breakdown occurs when the tip clearance vortex interacts with the passage shock at near-stall conditions. It was indirectly implied that vortex breakdown causes stall inception in their investigations on transonic flow in a radially stacked rotor (NASA's Rotor 37). The results in Fig. 7 do not show similar behavior of the tip clearance vortex during stall inception. The tip clearance vortex originates near the leading edge from interaction between the incoming flow and flow coming over the blade tip. As the blade loading increases, the pressure gradient over the tip increases and the tip vortex moves further away from the blade after formation at the leading edge. The tip clearance core vortex also moves radially inward as it moves downstream. A projection of the tip clearance vortices onto an axial cross plane is shown in Fig. 8 for all three operating conditions. The black circular arc above the traces represents the machine casing. The vortices originate at the blade leading edge on the left and propagate in the circumferential direction to the right. At stall, the tip vortex moves radially inward more than at peak efficiency.

Figure 9 shows entropy contours at the blade tip and at 96% span, along with tip clearance vortex traces. Arrows identify low momentum regions near the casing, associated with high entropy. As shown in Figs. 7 and 9, the areas with low momentum fluid are not directly related to the trajectory of the tip clearance vortices.

Figure 10 shows velocity vectors colored by Mach number at the blade tip along with tip clearance vortex traces for all three operating conditions. Differences in the tip clearance vortex traces and velocity fields near the leading edge at different operating conditions are clearly illustrated in Fig. 10. At stall, like the zero clearance flow field at stall, a strong cross flow develops where the passage shock interacts with the blade boundary layer. This cross flow seems to carry low momentum fluid from the upstream endwall boundary layer. This accumulation of low momentum fluid increases flow blockage near the pressure side of the leading edge and prevents incoming flow from entering the passage in that region, as shown in Fig. 10c. Velocity vectors near the leading edge in Fig. 10c show that tip clearance flow spills into the adjacent blade passage from the pressure side of the leading edge due to the blockage of this low momentum area.

Attempts were made to trace upstream to find the origins of the low momentum areas. Figure 11 shows calculated Mach number contours at 96% span and at the blade tip section at the stall condition. Three-dimensional particle traces (in blue) were released from the low momentum areas at those spanwise locations and traced both upstream and downstream. As shown in Fig. 11, the accumulation of the low momentum area is not the result of any breakdown of the tip clearance vortex. In some tangential locations, the endwall boundary layer extends nearly 5% of the blade span into the flow field, as shown in Fig. 7. The low momentum area at 96% span is formed by fluid coming from the upstream casing boundary layer. This fluid moves radially inward and wraps around the core vortex near the shock surface. As shown in Fig. 11a, this fluid changes flow direction sharply around the core vortex. Negative axial velocity components are commonly observed at this span. Traces from the low momentum area at the blade tip section show that the low momentum area is formed by fluid that crosses the blade tip about 40-50% chord from the leading edge. This fluid passes over the tip clearance vortex and the low momentum area is formed near the pressure side of the blade beyond the tip clearance vortex. This fluid also follows the cross flow direction observed at the blade tip in Fig. 10c. The regions with low momentum fluid inside the casing boundary layer are formed primarily with fluid from the upstream casing boundary layer and particles crossing over the tip gap downstream of the leading edge. Figure 12 shows the overall structure of the tip clearance flow at the stall condition with particle traces released from three radial locations in the tip gap. The tip core vortex is formed by fluid originating near the leading edge of the blade tip section. Fluid originating near the passage shock leg on the blade suction side near the tip travels above the core vortex and forms the low momentum area. Most of the fluid from the

leading edge to the shock leg moves radially downward and stays within the blade passage. Some of the fluid at mid-gap from the shock leg to the trailing edge passes through the tip clearance of the adjacent blade, resulting in so-called double leakage. For the current forward-swept rotor, formation of the low momentum area near the pressure side of the blade near the casing and the resulting large blockage are not caused by the breakdown of the tip clearance vortex.

### **Flow Structure with Partial Tip Clearance**

To examine the origin and the influence of the strong cross flow arising from the interaction of the passage shock and the blade suction surface, a flow field with zero tip clearance on the aft 60% of the chord was numerically simulated. In Fig. 13, Mach number contours, particle traces for the tip clearance vortex, and traces for the low momentum area are shown for the near-stall condition. Computed velocity vectors at the blade tip section are shown in Fig. 14. Because the tip gap is zero where the passage shock interacts with the suction surface, no particles can flow over the blade tip toward the low momentum area. However, strong cross flow still develops as in the zero clearance case and flow particles from the upstream endwall boundary layer accumulate to create the low momentum area. As shown in the rotor performance maps of Fig. 2, the partial blockage of the tip gap extends the operating range of the rotor somewhat without any increase in efficiency, which indicates that most of the influence of the tip gap flow is due to the portion on the forward part of the blade.

### **Oscillation of Passage Shock and Tip Clearance Vortex**

Previous studies (for example, Copenhaver et al. [1997]) have shown that the passage shock oscillates over as much as 2% of the blade chord in a similar transonic compressor. Zierke et al. [1994] also measured unsteady movement of a tip clearance vortex in their experimental study of a low speed axial pump. In the current study, unsteady calculations with a time step of 0.0000125 sec. were performed for the nominal tip clearance at the near-stall condition. Figure 15 shows Mach number contours and the tip clearance vortex at three different instants in time. The passage shock can be seen to oscillate due to the interaction between the passage shock and the blade boundary layer, and any resulting vortex shedding. As the shock oscillates, the cross flow originating at the shock leg also oscillates and the tip clearance vortex changes its trajectory. However, the core vortex does not break down. The flow unsteadiness observed near the stall condition in this transonic rotor is not due to the breakdown of the tip clearance vortex. The unsteadiness in the current compressor rotor is mainly due to shock/boundary-layer interaction and any resulting vortex shedding. Krause [2002] and Thomer et al. [2002] concluded that the formation of a stagnation point is required for the onset of slender vortex breakdown. From their study, it seems that the tip clearance vortex should interact with a normal shock for vortex breakdown to occur. As shown in this study, the tip clearance vortex interacts with an oblique shock in both the

blade-to-blade and spanwise directions. This might contribute to the fact that the tip clearance vortex does not break down for the current rotor, even during the early stall initiation process.

## CONCLUDING REMARKS

Detailed flow features near the casing in a forward-swept transonic compressor rotor were studied with steady and unsteady three-dimensional viscous flow analyses. The main objectives of the study were to understand the roles played in stall inception by flow interactions between the tip clearance flow, the passage shock, and the blade and endwall boundary layers. The following conclusions were drawn.

1. The tip clearance vortex, which is formed by fluid crossing the tip gap very close the leading edge, moves away from the suction side and radially inward as the rotor operates closer to the stall condition
2. The tip clearance vortex does not break down, even for rotor operation in the stalled condition.
3. A low momentum area occurs immediately downstream of the passage shock and very close to the casing. The tip clearance vortex passes under this low momentum area. The low momentum area is formed with fluid from the upstream endwall boundary layer and is located much closer to the pressure side of the blade than is the tip clearance vortex. The formation of this low momentum region is not directly related to the tip clearance vortex or any possible breakdown of the tip clearance vortex. This blockage area moves further toward the pressure side of the blade for near-stall operation. Eventually, this blockage forces tip clearance flow to spill into the adjacent blade passage from the pressure side, which initiates stall inception.
4. Even though the tip clearance vortex does not break down, the flow field becomes unsteady due to shock oscillation. The tip clearance vortex subsequently oscillates, but without any breakdown.
5. Further studies are necessary to find ways to control the flow structure near the casing, especially the formation of the low momentum area, for efficient operation with a wide stall margin.

## ACKNOWLEDGMENTS

The authors would like to acknowledge the contribution of J. Loellbach of ICOMP in preparing the illustrations.

## REFERENCES

Adamczyk, J. J., Celestina, M. L., and Greitzer, E. M., 1993, "The Role of Tip Clearance in High-Speed Fan Stall," *ASME Journal of Turbomachinery*, Vol. 115, pp. 28-38.

Chima, R. V., 1998, "Calculation of Tip Clearance Effects in a Transonic Compressor Rotor," *ASME Journal of Turbomachinery*, Vol. 120, pp. 131-139.

Copenhaver, W. W., Mayhew, E. R., Hah, C., and Wadia, A. R., 1996, "The Effects of Tip Clearance on a Swept Transonic Compressor Rotor," *ASME Journal of Turbomachinery*, Vol. 118, pp. 230-239.

Copenhaver, W. W., Puterbaugh, S. L., Hah, C., 1997, "Unsteady Flow and Shock Motion in a Transonic Compressor Rotor," *AIAA Journal of Propulsion and Power*, Vol. 13, pp. 17-23.

Hah, C., Copenhaver, W. W., Puterbaugh, S. L., and Wadia, A. R., 1998, "Control of Shock Structure and Secondary Flow Field Inside Transonic Compressor Rotors Through Aerodynamic Sweep," *ASME Paper 98-GT-561*.

Hah, C and Loellbach, J., 1999, "Development of Hub Corner Stall and its Influence on the Performance of Axial Compressor Blade Rows," *ASME Journal of Turbomachinery*, Vol. 121, No. 1, pp. 67-77.

Hah, C. and Rabe, D. C., 2001, "Role of Tip Clearance Flows on Flow Instability in Axial Flow Compressors," *ISABE Paper 2001-1223*.

Hah, C. and Wennerstrom, A. J., 1991, "Three-Dimensional Flow Fields Inside a Transonic Compressor with Swept Blades," *ASME Journal of Turbomachinery*, Vol. 113, No. 1, pp. 241-251.

He, L. and Ismael, J. O., 1997, "Computations of Blade Row Stall Inception in Transonic Flows," *ISABE Proceedings*, pp. 697-707.

Hoffman, W. H. and Ballman, J., 2003, "Some Aspects of Tip Vortex Behavior in a Transonic Turbocompressor," *ISABE Paper 2003-1223*.

Krause, E., 2002, "Axial Flow in Slender Vortices," *Proceeding of Fifth World Congress on Computational Mechanics*.

Law, C. H. and Wadia, A. R., 1993, "Low Aspect Ratio Transonic Rotors, Part 1: Baseline Design and Performance," *ASME Journal of Turbomachinery*, Vol. 115, pp. 218-225.

Rabe, D. C., and Hah, C., 2002, "Application of Casing Circumferential Grooves for Improved Stall Margin in a Transonic Axial Compressor," *ASME Paper GT-2002-30641*.

Schlechtriem, S. and Loetzerich, M., 1997, "Breakdown of Tip Leakage Vortices in Compressors at Flow Conditions Close to Stall," *ASME Paper 97-GT-41*.

Suder, K. L., and Celestina, M. L., 1994, "Experimental and Computational Investigation of the Tip Clearance Flow in a Transonic Axial Compressor Rotor," *NASA TM-106711*.

Thomer, O., Klass, M., Schroeder, W., and Krause, E., 2002, "Interaction between Longitudinal Vortices and Normal and Oblique Shocks," Proceedings of Fifth World Congress on Computational Mechanics.

Van Zante, D. E., Strazisar, A. J., Wood, J. R., Hathaway, M. D., Okiishi, T. H., 2000, "Recommendations for Achieving Accurate Numerical Simulation of the Tip Clearance Flows in a Transonic Compressor Rotor," ASME Journal of Turbomachinery, Vol. 122, pp. 733-742.

Wadia, A. R. and Law, C. H., 1993, "Low Aspect Ratio Transonic Rotors, Part 2: Influence of Location of Maximum Thickness on Transonic Compressor Performance," ASME Journal of Turbomachinery, Vol. 115, pp. 226-239.

Wadia, A. R., Szuch, P. N., and Crall, D., 1997, "Inner Workings of Aerodynamic Sweep," ASME Paper 97-GT-401.

Wennerstrom, A. J. and Puterbaugh S. L., 1984, "A Three-Dimensional Model for the Prediction of Shock Losses in Compressor Blade Rows," ASME Journal of Engineering for Gas Turbines and Power, Vol. 106, pp. 295-299.

Yamada, K, Furukawa, M., Inoue, M., and Funazaki, K., 2003, "Numerical Analysis of Tip Leakage Flow Field in a Transonic Axial Compressor Rotor," IGTC Paper 2003-095.

Zierke, W. C., Straka, W. A., and Taylor, P. D., 1993, "The High Reynolds Number Flow Through an Axial-Flow Pump" The Pennsylvania State University/ARL Technical Report No. TR93-12.

**Table 1. Rotor Key Design Parameters.**

Parameter	Value
Specific Flow	43.61 lbm/sec-ft <sup>2</sup>
Corrected Tip Speed	1500 ft/sec
Stage Pressure Ratio	1.92
Inlet Corrected Flow	61.81 lb/sec
Measured Stage Efficiency	0.8764
Inlet Radius Ratio	0.312
Tip Diameter	17 in
Number of Blades	20
Mean Aspect Ratio	1.32
Average Solidity	2.3

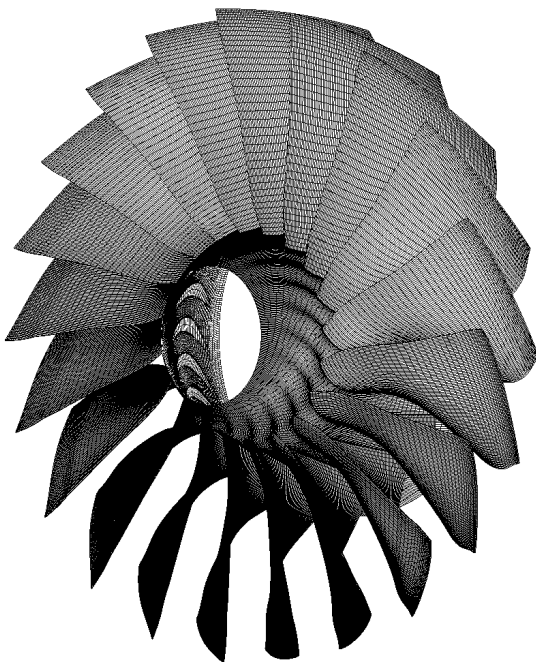
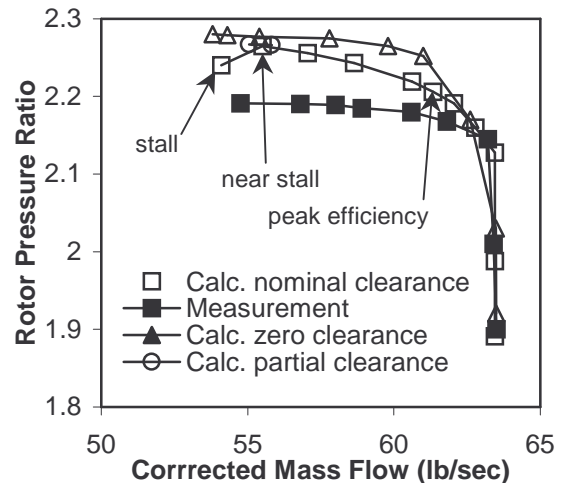
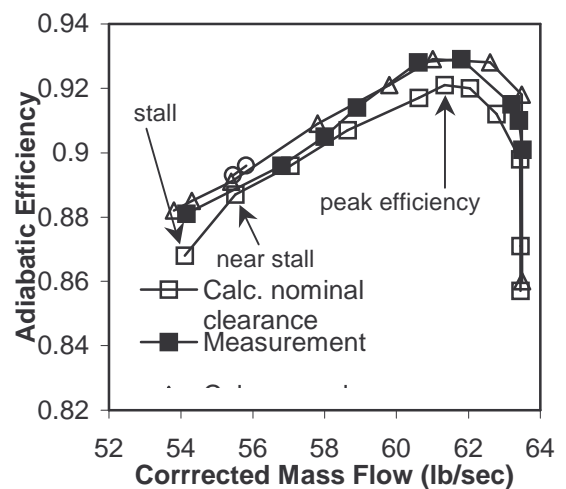


**Figure 1. Computational grid.**



**(a) rotor pressure ratio**



**(b) rotor efficiency**

**Figure 2. Measured and calculated rotor performance maps.**

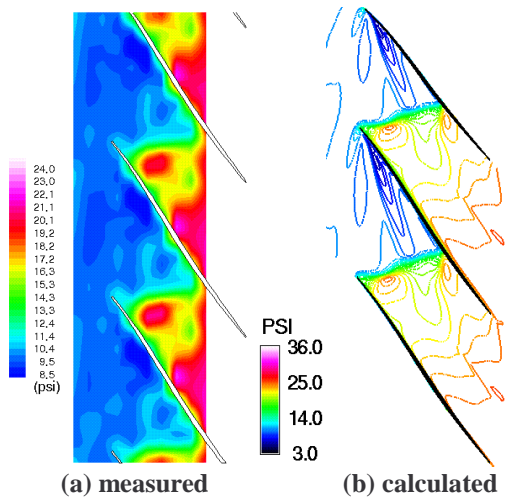


Figure 3. Comparison of measured and calculated shroud static pressure at peak efficiency.

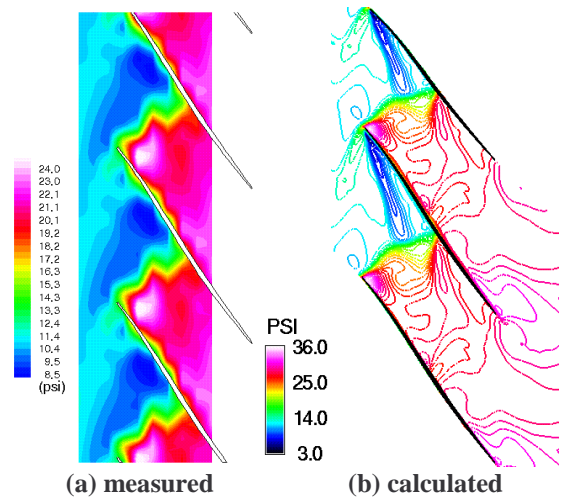


Figure 4. Comparison of measured and calculated shroud static pressure at near-stall condition.

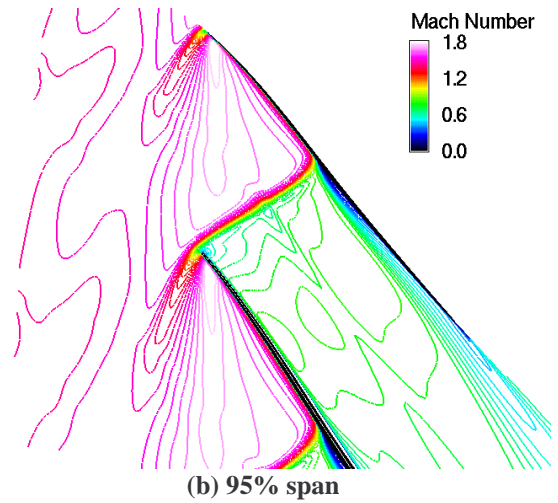
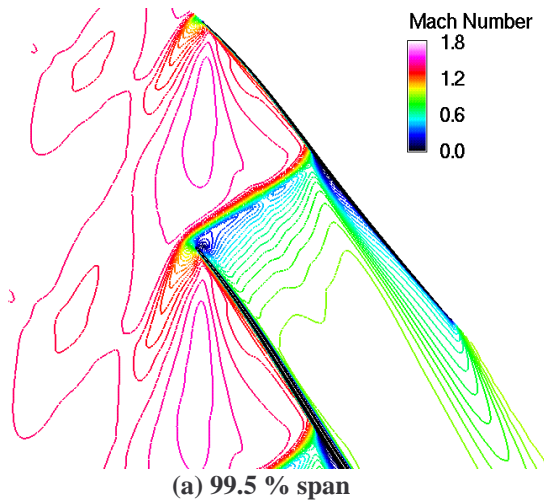


Figure 5. Mach number contours for zero clearance case at near-stall condition.

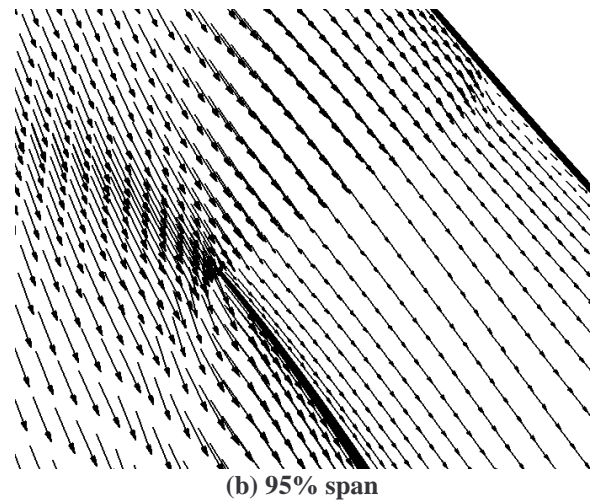
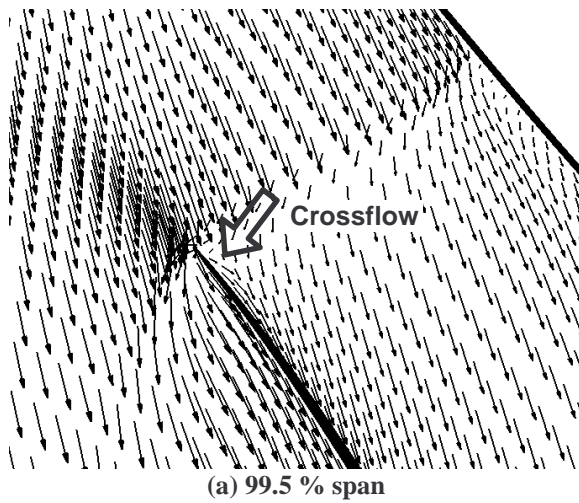
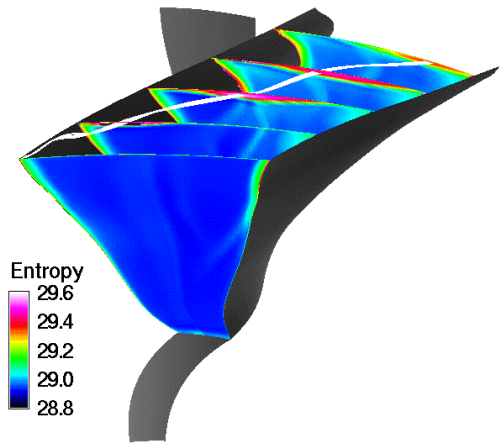
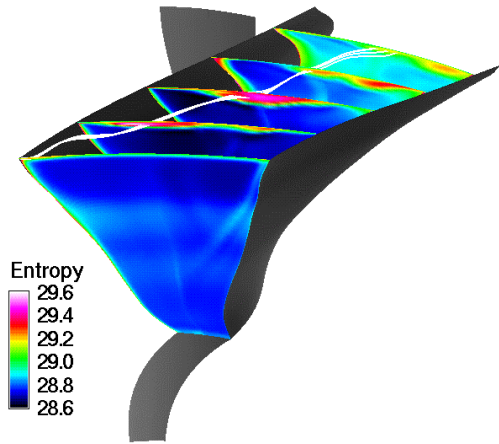


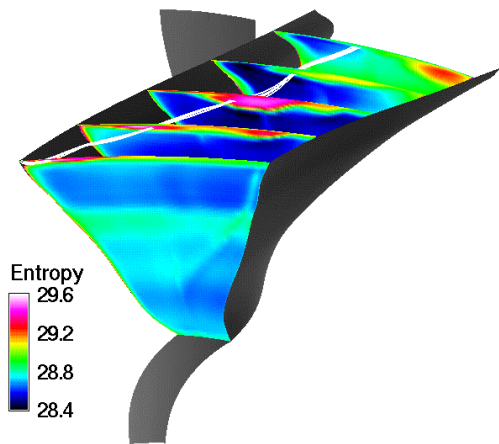
Figure 6. Velocity vectors for zero clearance case at near-stall condition.



(a) peak efficiency condition



(b) near-stall condition



(c) stall condition

Figure 7. Tip vortex traces and entropy on cross planes.

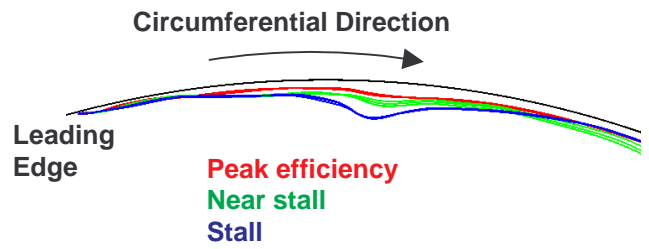
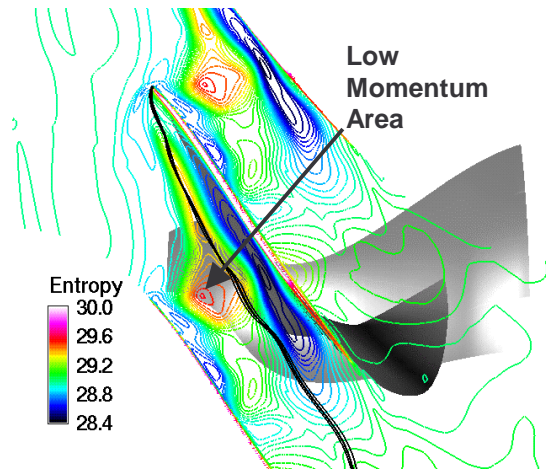
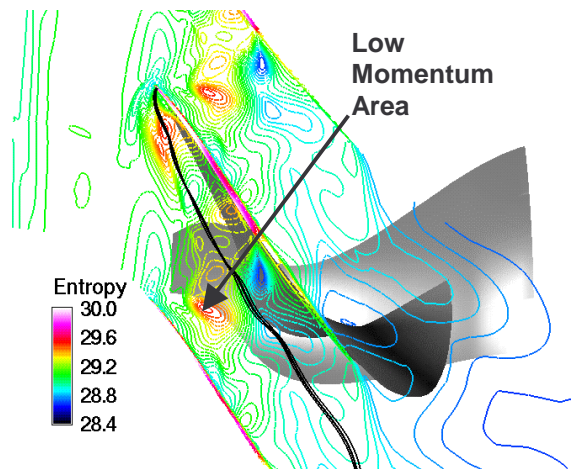


Figure 8. Radial migration of tip vortices at peak efficiency, near-stall, and stall conditions.

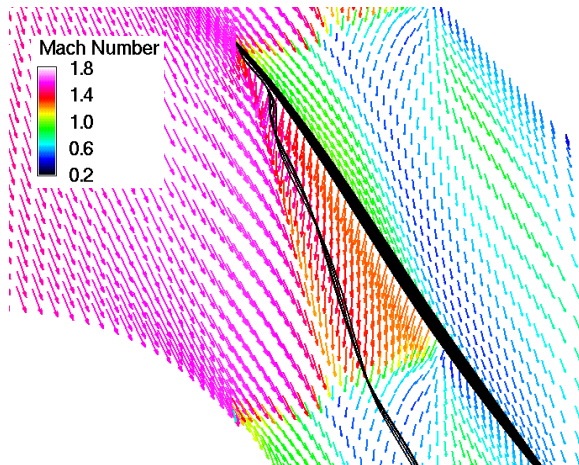


(a) entropy at 96% span

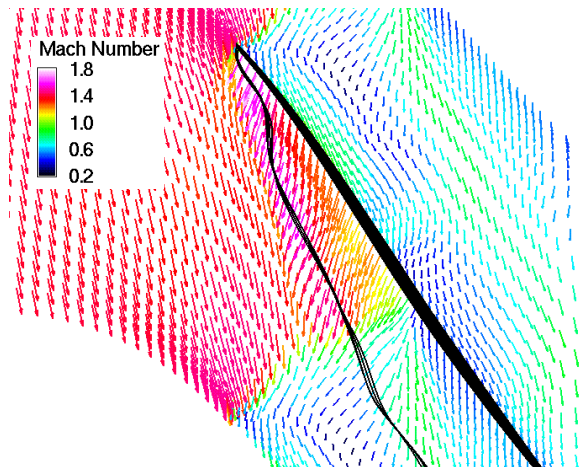


(b) entropy at blade tip

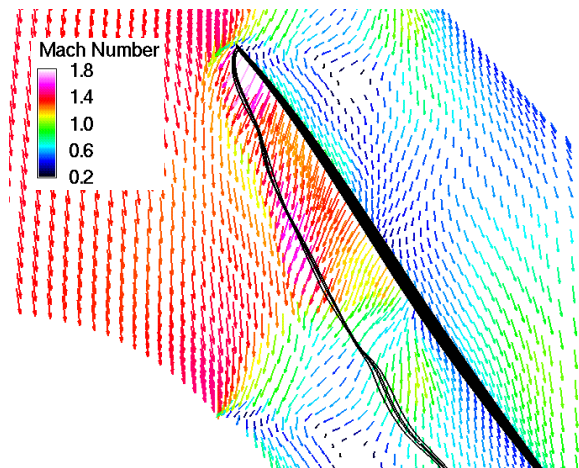
Figure 9. Tip vortex traces and entropy contours at stall condition.



(a) peak efficiency condition

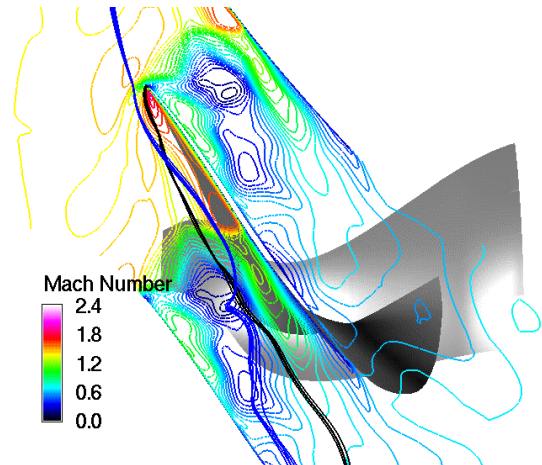


(b) near-stall condition

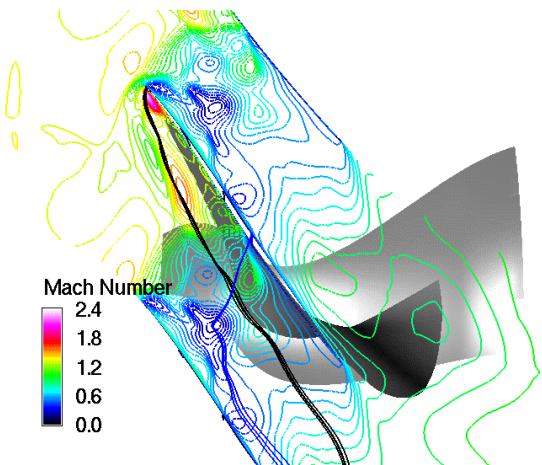


(c) stall condition

Figure 10. Tip vortex traces and tip-section velocity vectors colored by Mach number.



(a) Mach number contours and low-momentum traces at 96% span



(b) Mach number contours and low-momentum traces at blade tip

Figure 11. Tip vortex traces, traces through low-momentum area, and Mach number contours at stall condition.

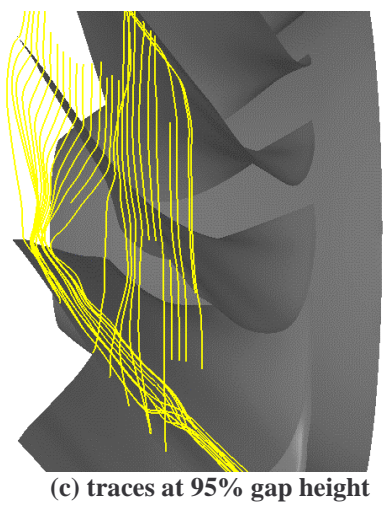
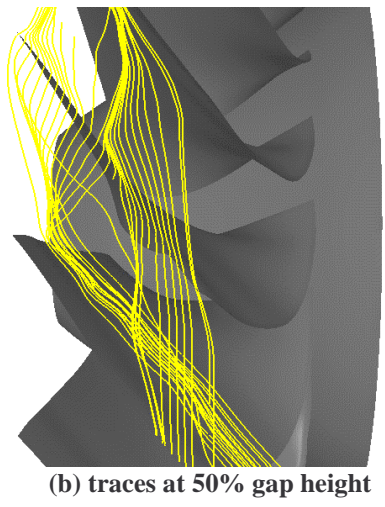
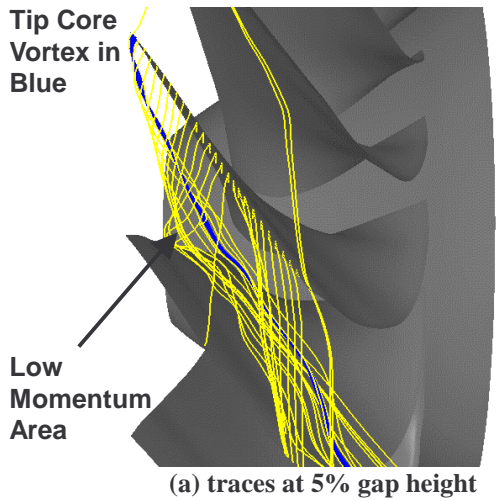


Figure 12. Three-dimensional structure of tip leakage flow.

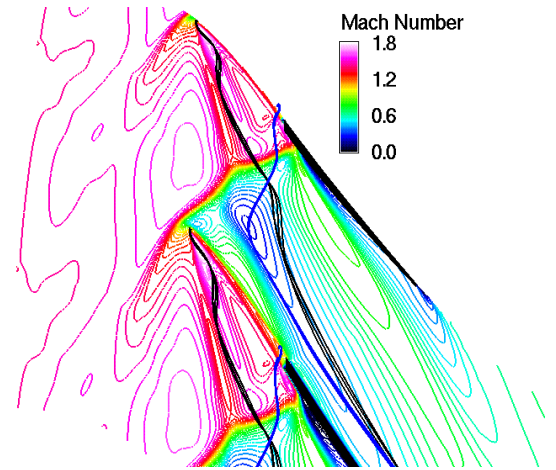


Figure 13. Tip vortex traces, traces through low-momentum area, and Mach number at blade tip, partial tip gap.

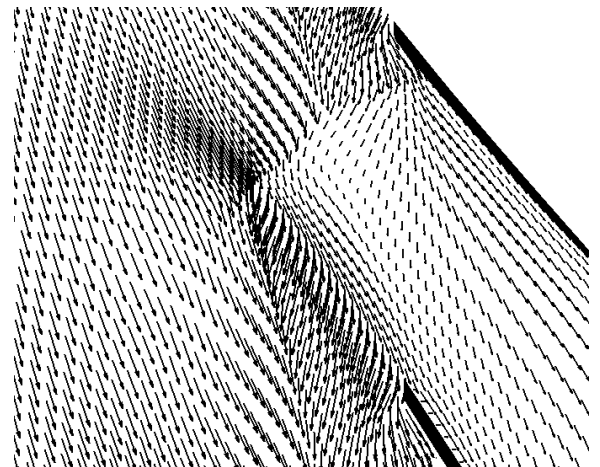
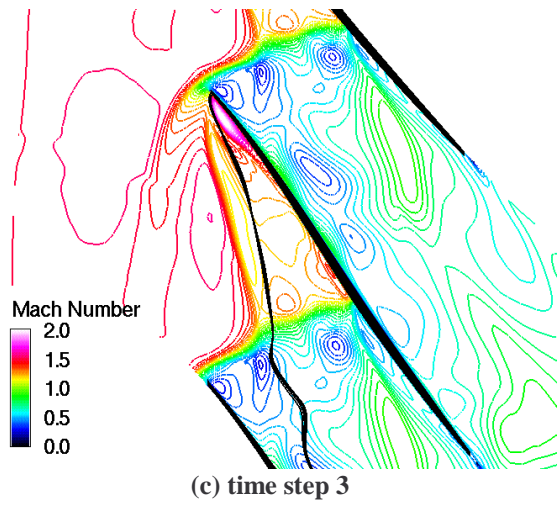
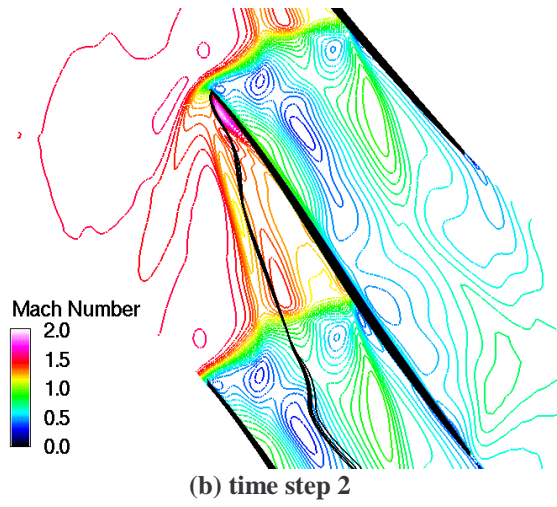
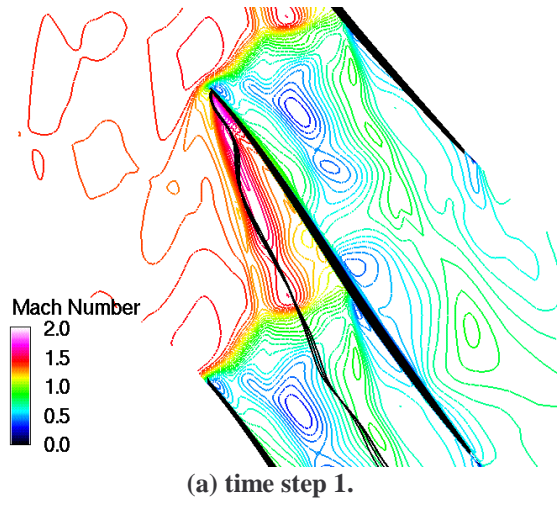


Figure 14. Velocity vectors at blade tip, partial tip gap.



**Figure 15. Instantaneous tip vortex traces and Mach number contours at the tip section, near stall condition, time step 3.**